



## Deposition and Evaluation of Protective PVD Coatings on Ferritic Stainless Steel SOFC Interconnects

V. I. Gorokhovskiy,<sup>a,\*</sup> P. E. Gannon,<sup>b</sup> M. C. Deibert,<sup>b</sup> R. J. Smith,<sup>b</sup> A. Kayani,<sup>b</sup>  
M. Kopczyk,<sup>b</sup> D. VanVorous,<sup>a</sup> Zhenguo Yang,<sup>c,\*</sup> J. W. Stevenson,<sup>c</sup>  
S. Visco,<sup>d,\*</sup> C. Jacobson,<sup>d</sup> H. Kurokawa,<sup>d</sup> and S. W. Sofie<sup>e</sup>

<sup>a</sup>Arcomac Surface Engineering, LLC, Bozeman, Montana 59715, USA

<sup>b</sup>Montana State University, Bozeman, Montana 59715, USA

<sup>c</sup>Pacific Northwest National Laboratory, Richland, Washington 99352, USA

<sup>d</sup>Lawrence Berkeley National Laboratory, Berkeley, California 94720, USA

<sup>e</sup>NASA-Glenn Research Center, Cleveland, Ohio 44135, USA

Reduced operating temperatures (600–800°C) of solid oxide fuel cells (SOFCs) may enable the use of inexpensive ferritic steels as interconnects. Due to the demanding SOFC interconnect operating environment, protective coatings are gaining attention to increase long-term stability. In this study, large area filtered arc deposition and hybrid filtered arc deposition-assisted electron beam physical vapor deposition technologies were used to deposit two-segment coatings with Cr-Co-Al-O-N-based bottom segment and Mn-Co-O top segment. The bottom segment serves as a diffusion barrier and bond segment, while the top segment is meant to increase electrical conductivity and inhibit Cr volatility. Coatings were deposited on ferritic steel and subsequently annealed in air for various time intervals. Surface oxidation was investigated using Rutherford backscattering spectrometry, scanning electron microscopy, and energy-dispersive spectrometry analyses. Cr volatilization was evaluated using a transpiration apparatus and inductively coupled plasma-mass spectrometry analysis of the resultant condensate. Electrical conductivity (area specific resistance, ASR), was studied as a function of time using the four-point technique. Significant improvement in oxidation resistance, Cr volatility, and ASR were observed in the coated versus uncoated samples. Transport mechanisms for various oxidizing species and coating diffusion barrier properties are discussed.

© 2006 The Electrochemical Society. [DOI: 10.1149/1.2266244] All rights reserved.

Manuscript submitted October 31, 2005; revised manuscript received June 5, 2006. Available electronically August 8, 2006.

Planar solid oxide fuel cells (SOFCs) are increasingly promising candidates for future energy conversion due to their inherently high efficiencies and decreasing environmentally sensitive emissions.<sup>1</sup> Typical anode-supported planar SOFC design and operation are described elsewhere.<sup>2</sup> During operation, the planar SOFC interconnect component realizes simultaneous dual atmosphere (wet reducing and oxidizing) exposure up to ~800°C. The interconnect/electrode and interconnect/seal interfaces must exhibit chemical, thermal-mechanical, and electrical stability throughout the desired SOFC stationary device lifetime of >40,000 h, while enduring a large number of thermal cycles.<sup>3</sup> High-temperature metallic alloys have received attention for use as intermediate-temperature (600–800°C) SOFC interconnects due to their higher relative toughness and formability and much lower costs compared to commonly used ceramic alternatives. Of particular interest are high Cr content, ferritic stainless steels, which exhibit compatible thermal expansion coefficients with other SOFC components, but form electrically resistive thermally grown oxide (TGO) scales when exposed to the complex SOFC operating gases. TGO scales can introduce adverse chemical and thermal-mechanical incompatibilities with adjoining SOFC components through deleterious species volatilization, interdiffusion, and thermal-mechanical stresses. A thorough investigation of several heat-resistant alloys concluded that, for improved oxidation resistance and electrical conductivity, either new alloys need to be developed or surface engineering of existing alloys is required.<sup>4</sup> Among the candidates in the former category is Crofer 22 APU, a ferritic stainless steel (20–24%Cr), with engineered additions of Mn, Ti, and La (available from ThyssenKrupp VDM).<sup>5</sup> This special high-temperature stainless steel is characterized by the formation of a stable and electrically conductive Cr-Mn oxide surface layer during SOFC cathode gas-phase exposure. However, continued TGO scale growth (dominated by an underlying Cr<sub>2</sub>O<sub>3</sub> layer) during extended exposures may create increased electrical resistance and other SOFC incompatibilities.<sup>6</sup>

The present work is focused upon further enhancement of Crofer 22 APU by depositing surface coatings using large area filtered arc

deposition (LAFAD) or hybrid filtered arc deposition-assisted e-beam physical vapor deposition (FAD-EBPVD) processes.<sup>7,8</sup> Various single and dual-segment LAFAD and FAD-EBPVD coatings from the Co-Mn-Cr-Al-O-N system have been applied to sample coupons of Crofer 22 APU alloy in an attempt to improve its SOFC-interconnect performance characteristics. This research is aimed toward understanding the influence of coating characteristics (thickness, structure, phase, and chemical composition) on long-term thermal-mechanical and chemical stability of interconnect/cathode interface during SOFC exposure. Related research in this area includes deposition of conductive oxide and nitride coatings using various techniques.<sup>9–14</sup>

### Experimental

*Coating architectures and plasma vapor deposition processes.*—A broader goal of this research is to enable the use of inexpensive alloys for SOFC interconnects by developing a coating material system and deposition process to ensure electrical, chemical, and thermal-mechanical compatibility with other SOFC stack components, throughout the device's lifetime. Toward this end, the dual-segment coating approach, illustrated in Fig. 1, has been investigated.

The use of coatings to improve oxidation resistance on metal alloys has been known for many years. The LAFAD Co-Cr-Al-O-N bottom-segment coating system was selected for this study due to previously demonstrated oxidation and wear resistance at temperatures up to 900°C.<sup>12–14</sup> Nanolayered structures consisting of alternating AlON and CoCrON sublayers have been investigated with the goal of revealing the application-specific efficacy of this surface treatment.

The FAD-EBPVD Mn<sub>1.5</sub>Co<sub>1.5</sub>O<sub>4</sub> system was investigated as a top segment coating because of its SOFC cathode compatibility, its recently reported success in reducing ASR, as well as its anticipated reduction in Cr volatilization.<sup>15–17</sup>

Two primary coating architectures were investigated: one with the top Mn<sub>1.5</sub>Co<sub>1.5</sub>O<sub>4</sub> segment only (~2 μm), and one with both the bottom CoCrAlON bond coating segment and top Mn<sub>1.5</sub>Co<sub>1.5</sub>O<sub>4</sub> segment present (~4 μm). Results from long-term (>2000 h) oxidation in air at 800°C, ASR, and Cr volatility from the two unique

\* Electrochemical Society Active Member.

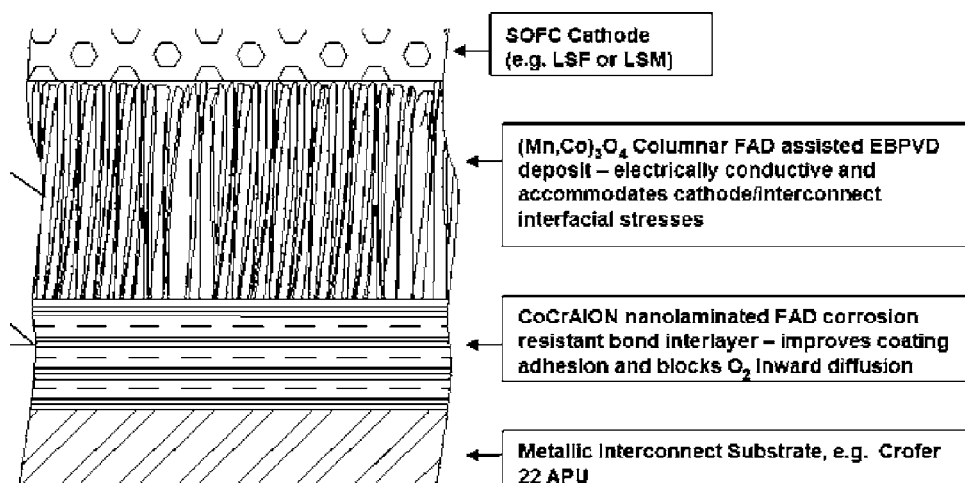


Figure 1. Dual segment, hybrid coating approach.

coated samples, in addition to uncoated samples are presented here, together with an interpretation of the significance of these results.

The single and dual-segment coatings were deposited on  $\sim 1.6 \text{ cm}^2 \times 1 \text{ mm}$  thick mechanically lapped and polished (50–80 nm nominal roughness by LapRight, Inc.) substrate coupons of Crofer 22 APU by Arcomac Surface Engineering, LLC using patented filtered arc plasma source ion deposition (FAPSID) technology.<sup>7</sup> The universal FAPSID surface engineering system employs a hybrid combination of LAFAD plasma sources with conventional e-beam evaporators, unbalanced magnetrons, thermal resistive evaporators, and low-pressure chemical vapor deposition (CVD) sources all integrated in the one plasma processing chamber layout (Fig. 2). This allows for deposition of virtually any PVD and low-pressure CVD coatings in highly ionized filtered arc plasma environment. The LAFAD dual-filtered arc plasma source utilizes rectangular plasma-guide chamber with two rectangular deflecting coils installed on opposite sides, with electron beam evaporators within the chamber, as shown in Fig. 2. In this design, two primary cathodic arc sources utilizing Cr/Co (6%) and Al (99.9%) targets are placed opposite each other on the sidewalls of the plasma-guide chamber, surrounded by rectangular deflecting coils, and separated by an anodic baffle. The LAFAD vapor plasma source uses a super-

imposed deflecting magnetic field to turn the metal ion flow 90° toward the deposition chamber and substrates. More massive droplets of target material and ionized metal vapor atoms follow straight trajectories and are captured on baffles, resulting in droplet-free 100% ionized metal vapor plasma yield for deposition of CoCrAlON bottom-coating segment. A set of scanning magnetic coils allows the ion plasma jet to be rastered, thereby promoting uniform coverage of large surface areas.<sup>8</sup> When the deflecting magnetic field coils are off, the LAFAD source can be employed as an effective, large area plasmatron, ionizing vapors from other conventional sources and the gaseous environment within the chamber. During the FAD-EBPVD deposition of the  $\text{Mn}_{1.5}\text{Co}_{1.5}\text{O}_4$  upper-coating segment, the LAFAD source is used as a powerful emitter of electrons, effectively ionizing the  $\text{Mn}_{1.5}\text{Co}_{1.5}\text{O}_4$  vapor and reactive oxygen gas atmosphere, aiming to densify the resultant coating. In this gaseous plasma ionizing mode the deflecting magnetic subsystem of the filtered arc source is deactivated and the cathodes of the primary arc sources serve as electron emitters while the distant auxiliary anode accepts the electron current. Ionization rate in the auxiliary arc plasma discharge reaches up to 50%.<sup>8</sup> The metal vapor flow from the e-beam evaporator is also substantially ionized via collisions with the auxiliary arc electrons.

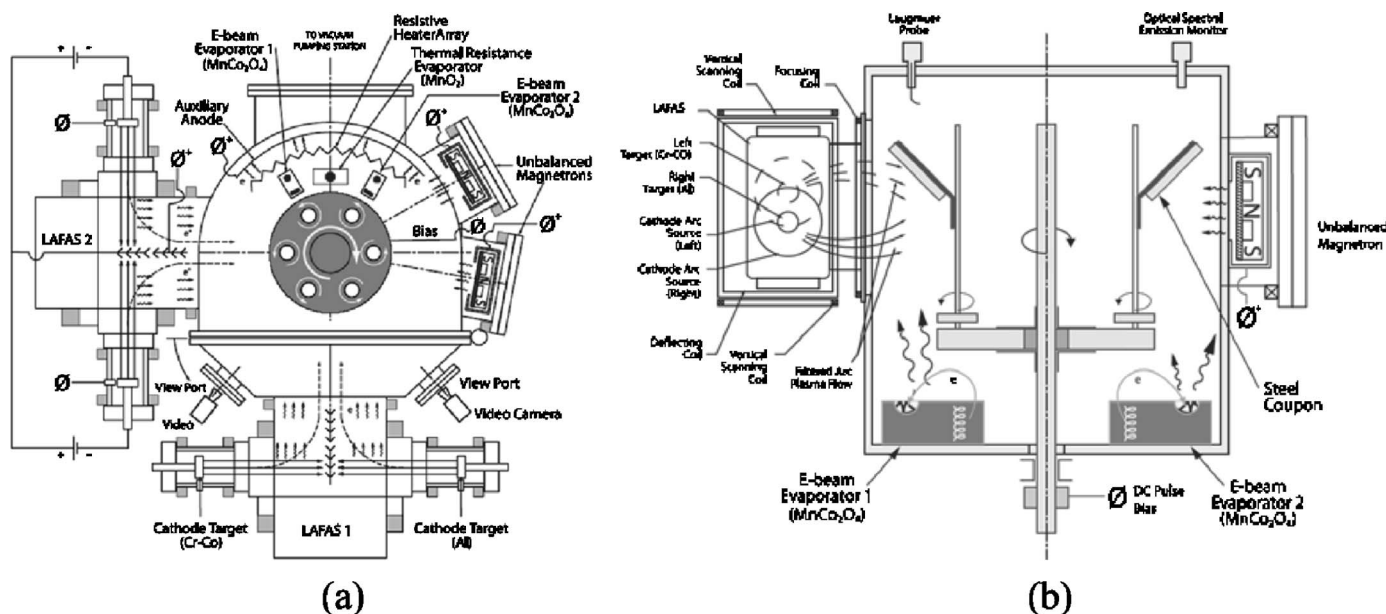


Figure 2. Schematic illustration of the FAPSID surface engineering system, showing (a) top view; and (b) side view.

The substrates were mounted on pedestals distributed about the outer rim of a rotating carousel in the FAPSID chamber. Substrate temperature during deposition of the bottom CoCrAlION coating segment was about 500°C. Substrates were first cleaned in an Ar plasma at  $8 \times 10^{-2}$  Pa for 20 min, followed by 2 min of high voltage ( $-1000$  V bias) Co-Cr-Al metal ion bombardment stage in Ar at  $2 \times 10^{-2}$  Pa. Cr-Co and Al ions were then deposited in an 60% O<sub>2</sub>:40%N<sub>2</sub> reactive gas atmosphere with 3% Ar addition at  $\sim 4 \times 10^{-2}$  Pa. In addition, the preliminary experiments were conducted with different O/N ratios to study oxidation kinetics of these CrAlION-based coatings. The applied medium frequency (MF) substrate bias was set at  $-300$  V with frequency of 40 kHz. With both target sources on and substrate rotation engaged, the substrates were successively exposed to Cr/Co, then Al ions, in a mixed O<sub>2</sub>/N<sub>2</sub> reactive gas atmosphere, resulting in nanometer-size bilayers of CrCoO/N/AlO/N. Thickness of the individual bilayers in the coating was controlled by the rotation speed of the carousel, deposition time, and total coating thickness, and was estimated at  $\sim 2.1$  nm for the coatings considered here. The FAD-EBPVD Mn<sub>1.5</sub>Co<sub>1.5</sub>O<sub>4</sub> upper-segment coating was deposited by evaporating a sintered Mn<sub>1.5</sub>Co<sub>1.5</sub>O<sub>4</sub> spinel target pellet using a standard 6 kW electron beam rastered over the target, with an emission current of  $\sim 300$  mA. The pressure during the FAD-EBPVD process was  $\sim 4 \times 10^{-2}$  Pa in a reactive oxygen gas atmosphere with 3% Ar addition. During the evaporation, the LAFAD plasma source was set in ionization auxiliary arc discharge mode (deflecting magnetic field off), with an auxiliary arc current of  $\sim 100$  A. The substrate bias during deposition of this layer was set at  $-60$  V dc.

**Coating properties characterization.**—Coating adhesion was assessed by means of the Mercedes indentation test using a Rockwell C indenter with  $\sim 150$  kgf load. Radial cracks surrounding the indentation indicate good coating adhesion. Radial cracks with localized delamination indicate fair adhesion, and concentric cracks around the indentation with large area delamination indicate poor coating adhesion.<sup>18</sup>

Oxidation of the sample coupons (in Bozeman, MT air) was carried out using a standard furnace operated with no control of humidity or air circulation. Measurements of area specific resistance (ASR) were made in air at 800°C using standard procedures with Ag paste electrodes on preoxidized samples as a function of time and temperature for coated and uncoated Crofer 22 APU coupons.<sup>2,4</sup>

Subsequent to varying exposure times, sample cross sections for microscopic analysis were prepared by epoxy-mounting, sectioning, and polishing. Scanning electron microscopy/energy dispersive spectrometry (SEM/EDS) analysis was performed using a JOEL SEM model S4700.

Ion beam analysis of the coated samples was performed using the 3 MV tandem accelerator at the Environmental Molecular Sciences Laboratory (EMSL) at Pacific Northwest National Laboratory (PNNL) in Richland, WA, and the 2 MV van de Graaff accelerator at Montana State University. The latter was used for beams of He<sup>+</sup> and H<sup>+</sup> up to 2 MeV, while the former provided higher energy He<sup>+</sup> beams to analyze thicker coatings, and d<sup>+</sup> beams for nuclear reaction analysis of the O and N concentrations, using the <sup>14</sup>N(d,p)<sup>15</sup>N and <sup>16</sup>O(d,p)<sup>17</sup>O reactions. Spectra were typically collected after total oxidation periods of 1, 4, 9, 16, and 25 h at 800°C in lab air with no control of humidity. The samples were removed from the oven for ion beam analysis, and were thus subjected to thermal cycling at a rate of  $\sim 25$ °C/min that might have adversely affected the coatings. Composition profiles were determined by comparing SIMNRA computer simulations of the spectra with the original data.<sup>19,21</sup>

Cr volatility was investigated using a transpiration apparatus developed at Lawrence Berkeley National Laboratory. To prevent Cr volatility from the uncoated side of the coated coupons, all samples (including uncoated) were first electroplated with  $\sim 50$  μm Ni on one (uncoated) side (Omni Metal Finishing, Inc.). The samples were preoxidized in air at 800°C for 2 h prior to 24 h exposure to

200 sccm air with  $1 \times 10^4$  Pa H<sub>2</sub>O at 800°C. The condensate from the effluent gas was then analyzed for its Cr content using inductively coupled plasma-mass spectrometry (ICP-MS).

## Results and Discussion

Ion beam analysis was used to characterize the oxidation resistance and diffusion characteristics for several candidate bond coatings coming from the CoCrAlION system. Figure 3 shows the results for the effectiveness of a CrAlION bond coat, with no top coat and three different O/N ratios in the as-grown coatings. The surface of the coating is at the left side in each profile, and the steel substrate can be seen at the right with its characteristic high Fe concentration. The depth scale unit ( $1 \times 10^{15}$  atoms/cm<sup>2</sup>) is characteristic of Rutherford backscattering spectrometry (RBS) measurements, and for this case corresponds to approximately 0.2 nm. The vertical scale is a percentage concentration, based on the assumption that the individual concentrations add to 100%. No measurement of hydrogen concentration was made for these coatings. The left column shows the composition for the three coatings as prepared with decreasing oxygen concentration from top to bottom. The O/N ratio for the coatings correlates well with the O/N partial pressure ratio in the chamber during growth. The right column shows the concentration profile for each sample after 25 h of oxidation at 800°C in a tube furnace with laboratory air.

On bare steel (without protective coating), oxygen activity at the surface is essentially the oxygen partial pressure in ambient air, i.e.,  $\sim 0.2$  atm, if disregarding water vapor or the surface boundary diffusion layer, which is quite thin at 800°C. Given a sufficient Cr concentration in the steel, Cr is selectively oxidized and forms an external Cr<sub>2</sub>O<sub>3</sub>-based scale. Once Cr<sub>2</sub>O<sub>3</sub> is thermally grown into a dense, continuous surface layer, the oxygen activity at the scale/steel interface decreases, and the scale growth slows down and enters into a steady state. During this state, the scale continues to grow by Cr outward diffusion and oxygen inward diffusion across the thermally grown scale, with the Cr inward transport often dominating and the growth following a parabolic relationship.<sup>22</sup> The continuous growth of the scale over long terms may lead to increased stress in the scale and in particular at the scale/steel interface, causing scale spallation and loss of protection against further environmental attack.

To improve the steel surface stability and resistance against environmental attack, protective coatings, such as a CoCrAlION, are applied onto the steel surface. First, CoCrAlION coatings act as a diffusion barrier to oxygen inward diffusion and preferably also to outward Cr diffusion. Assuming the protective coating entirely inhibits the outward Cr diffusion, it can be deduced that the scale growth beneath the coating is limited by the inward flux of oxygen.<sup>22</sup> Accordingly, the following relationship can be considered to describe the scale growth rate in the presence of protective diffusion barrier coating:  $v_{TGO} \sim P_{O_2}^{1/2} D_O(\text{CoCrAlION}) / (d_f)$ , where  $v_{TGO}$  is the growth rate of chromia TGO;  $P_{O_2}$  is partial pressure of oxygen on the scale/cathode interface;  $D_O(\text{CoCrAlION})$  is oxygen diffusion coefficient throughout the CoCrAlION coating; and  $d_f$  is coating thickness. A decreased inward flux of oxygen is expected to drastically mitigate the scale growth of the scale and thus to improve the surface stability of the steel. Second, the CoCrAlION coating is expected to serve as a barrier against Cr outward diffusion with and without additional top segment (Co,Mn)<sub>3</sub>O<sub>4</sub>, which serves exclusively as a Cr diffusion inhibitor. In the case of two-segment coating design, the bottom CoCrAlION coating acts as a bond coat that is expected to improve the adherence between the alloy substrate and the outside surface, which serves as a Cr barrier. To be effective and function well, the protective or bond coat has to be free from defects, such as open pores or cracks.

The CrAlION-based bond coats with different O/N ratios analyzed here behave very differently when subjected to the high-temperature oxidizing atmosphere (Fig. 3). Sample B9 with about 20% oxygen, as grown, lost almost all of the nitrogen in the coating, and shows only a small amount of Fe diffusion from the substrate

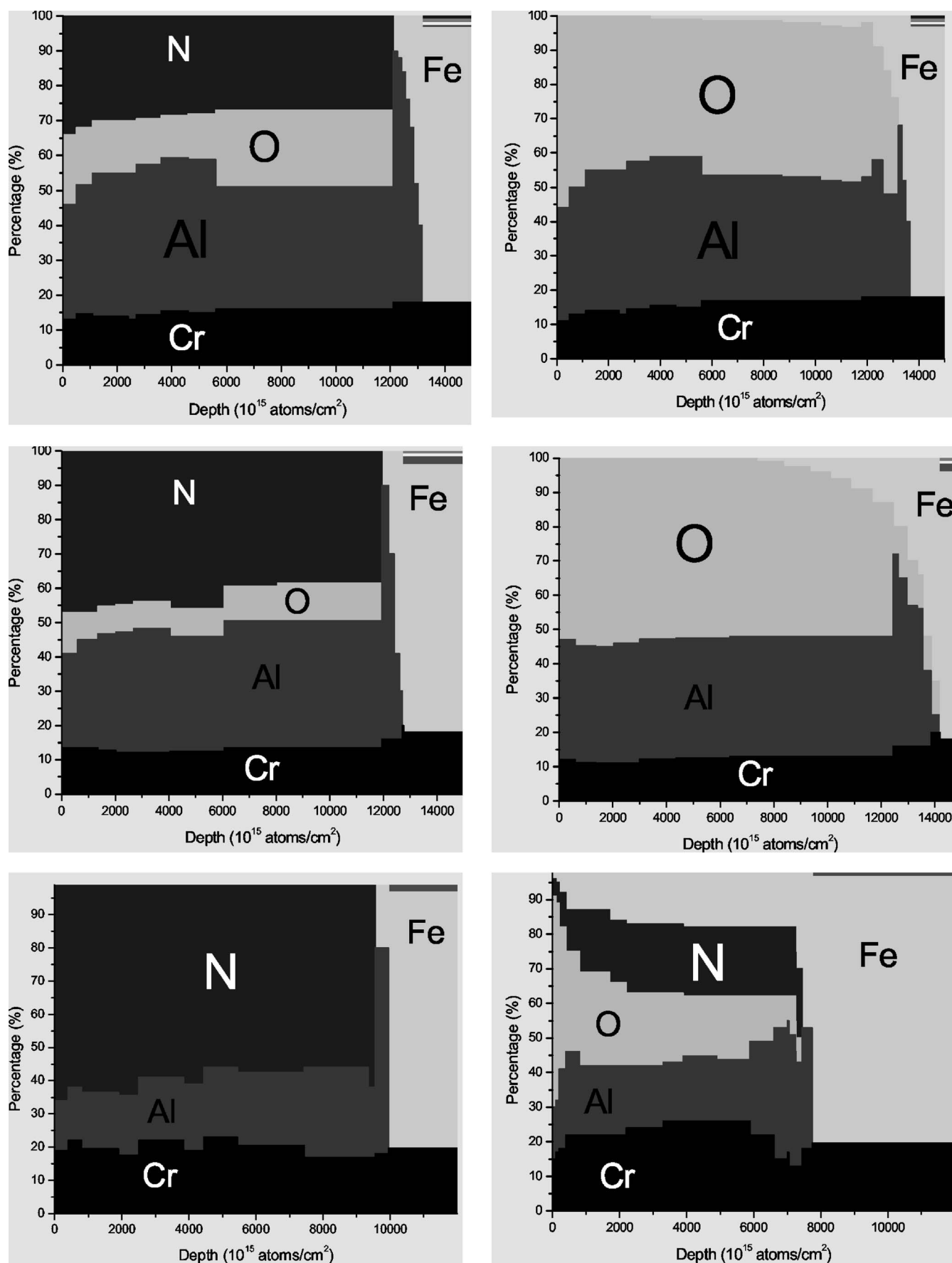


**Figure 3.** Profiles of concentration versus depth for three samples with (top to bottom) decreasing O/N ratios (left) before and (right) after 25 h oxidation at 800°C.

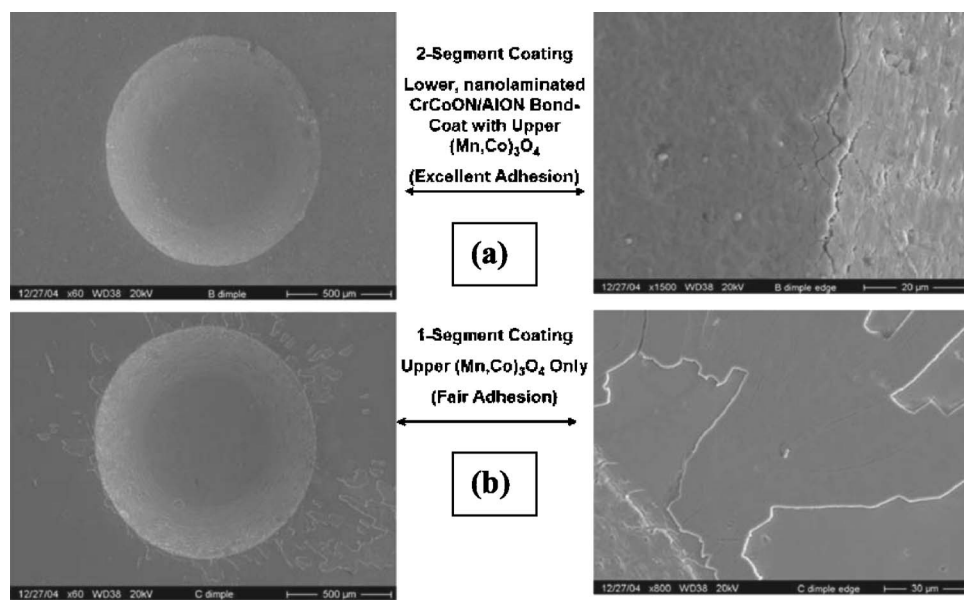


**Figure 4.** Adhesion (indentation) testing of as-deposited: (a) dual; and (b) single segment coatings on Crofer 22 APU.

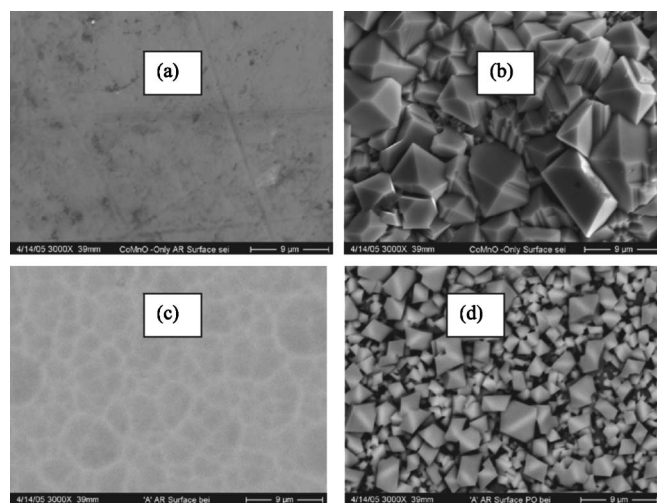
into the coating, although it did not diffuse all the way to the surface after 25 h. Coating C9 contains about 10% oxygen concentration as grown. In marked contrast to sample B9, the nitrogen in sample C9 is almost completely replaced by oxygen after only 1 h of heating at 800°C, and the coating is more susceptible to Fe diffusion from the substrate into the coating. However, this coating did not show any Fe at the surface after 25 h of heating. For coating D9 there is no oxygen in the as-grown sample. The nitrogen in the coating is gradually replaced by oxygen, and is completely lost after 25 h of heating at 800°C. Diffusion of Fe into the coating begins after only 1 h of heating, and Fe has reached the surface of the coating after 25 h of heating. Based on the above results, we conclude that introducing oxygen during the coating growth process creates more effective diffusion barriers that slow down the diffusion of Fe from the substrate into the coating. Synthetic formation of TGO scales during coating growth, rather than as a result of diffusion during subsequent oxidation, results in a more stable bond coat on these steel substrates.

Figure 4 shows adhesion testing results for as-deposited coatings: (a) dual segment (LAFAD CoCrAlON + FAD-EBPVD  $\text{Mn}_{1.5}\text{Co}_{1.5}\text{O}_4$ ) coating, and, (b) upper segment (FAD-EBPVD  $\text{Mn}_{1.5}\text{Co}_{1.5}\text{O}_4$ ) only coating. The radial crack propagation from the indentation in Fig. 4a demonstrates the excellent adhesion of the dual segment LAFAD CoCrAlON + FAD-EBPVD  $\text{Mn}_{1.5}\text{Co}_{1.5}\text{O}_4$  coating system. The localized area coating delamination near the indentation in Fig. 4b indicates only fair adhesion of the upper segment FAD-EBPVD  $\text{Mn}_{1.5}\text{Co}_{1.5}\text{O}_4$  coating, when deposited without the lower segment coating. These results indicate the substrate-coating adhesion promoting functionality of the dual segment coating architecture (with LAFAD CoCrAlON bond coating). This is likely because of the intense ion surface interaction during the initial coating deposition stage, resulting in significant ion implantation into the substrate and enhanced adhesion of the growing film.

On bare steel, scale spallation due to increased scale thickness is not an issue of compromised interfacial toughness. If the failure is just due to thickening, it is caused by an increase in stored elastic strain energy in the scale, due to an increase in scale volume. This causes the energy release rate driving scale debonding to become greater than the interfacial toughness (which is a measure of the interface's resistance to debonding). The ability of coatings to limit scale growth is critical and so deposition of defectless coatings is critical. Adding a coating to the chromia/steel system would generally increase the likelihood of spallation because of the addition of

another residually stressed layer on top of the growing chromia scale. If, however, the coating reduces chromia scale growth rates, the net effect could be no change or, if the scale growth is significantly reduced, the effect could be beneficial in preventing spallation. The latter can be achieved by optimizing coating thickness as well as toughness at the coating/scale interface.<sup>23</sup>

Figure 5 shows surface SEM images before and after high temperature oxidation in air at 800°C for over 2000 h. Figure 5a and b is an image of the single, upper segment filtered arc assisted EBPVD  $\text{Mn}_{1.5}\text{Co}_{1.5}\text{O}_4$  coating before and after 1,000 h oxidation in air at 800°C, respectively. Figure 5c and d is an image of the dual segment, LAFAD CoCrAlON + FAD-EBPVD  $\text{Mn}_{1.5}\text{Co}_{1.5}\text{O}_4$  coating system before and after 1,000 h oxidation in air at 800°C, respectively. The dual segment coating exhibits significantly finer surface microstructure compared to the single segment coating. This indicates a significant influence of the lower segment coating on the surface morphology and its evolution. Characteristics of the bond



**Figure 5.** Surface SEM images demonstrating coating recrystallization behavior: (a) as deposited, amorphous or ultrafine polycrystalline  $\text{Mn}_{1.5}\text{Co}_{1.5}\text{O}_4$  single segment coating; (b)  $\text{Mn}_{1.5}\text{Co}_{1.5}\text{O}_4$  single segment coating post-2000 h oxidation at 800°C; (c) as deposited, amorphous or ultrafine polycrystalline CoCrAlON +  $\text{Mn}_{1.5}\text{Co}_{1.5}\text{O}_4$  dual segment coating; and (d) CoCrAlON +  $\text{Mn}_{1.5}\text{Co}_{1.5}\text{O}_4$  dual segment coating post-2,000 h oxidation at 800°C.

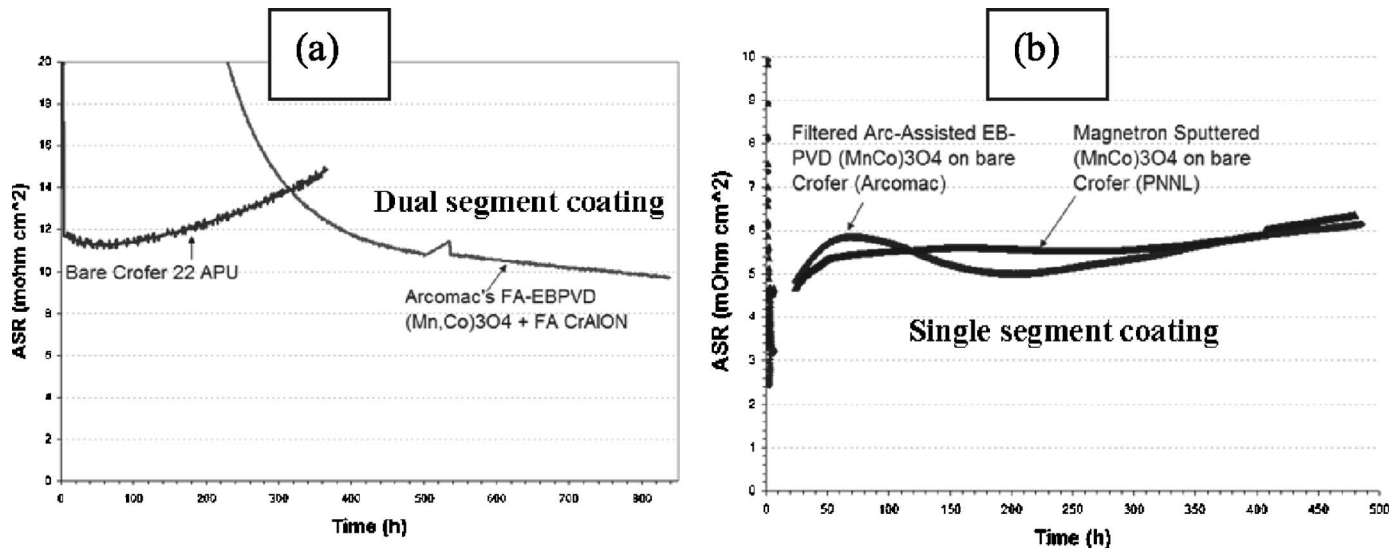


Figure 6. ASR testing results from PNNL.

segment coating, including its amorphous or ultrafine crystalline nature, in addition to its diffusion-barrier properties, may be responsible for this occurrence, and are the subject of ongoing investigations.

ASR testing was performed both at PNNL and MSU using Ag paste for electrical contact. Figure 6a shows PNNL data comparing uncoated and dual segment coated Crofer 22 APU. The ASR of the uncoated sample reaches a minimum after ~50 h, and rises steadily past 15 mΩ cm<sup>2</sup> after 300 h. The ASR values of the dual segment coating continue to decrease below 10 mΩ cm<sup>2</sup> after over 800 h of testing. The spike in this data maybe associated with the coating recrystallization process shown in Fig. 5, which is currently under investigation. Figure 6b shows ASR testing results of FAD-EBPVD deposited Mn<sub>1.5</sub>Co<sub>1.5</sub>O<sub>4</sub> compared to Mn<sub>1.5</sub>Co<sub>1.5</sub>O<sub>4</sub> deposited at PNNL using conventional magnetron sputtering. Differences in ASR behavior between these coating techniques are not significant, with both achieving a similar minimum ASR value of ~5 mΩ cm<sup>2</sup> with ASR slowly rising to ~6 mΩ cm<sup>2</sup> after ~400 h. As the process

times for conventional magnetron sputtered coating are an order of magnitude longer than that for FAD-EBPVD coating, the observation of ASR behavior similarity is promising. In addition, the FAD-EBPVD process may result in fewer coating defects and, therefore, improved diffusion-barrier properties compared with conventional coating deposition techniques. This would permit greater durability of the coating against the SOFC interconnect environmental attack.

ASR testing results at MSU from two coating systems and uncoated Crofer 22 APU are shown in Fig. 7. Spikes in the data represent thermal cycling events. The two coated samples display lower ASR values compared with uncoated Crofer 22 APU after ~550 h. ASR values for uncoated Crofer 22 APU continue to rise past 40 mΩ cm<sup>2</sup> after ~1,000 h, while coated samples display relatively stable ASR behavior, with values below ~25 mΩ cm<sup>2</sup> after ~2000 h. The upper segment coating alone had the lowest ASR values, while the dual segment coating exhibited the most ASR stability. The continued growth of a chromium-rich scale under the single, upper segment coating can explain the continued rise in ASR.

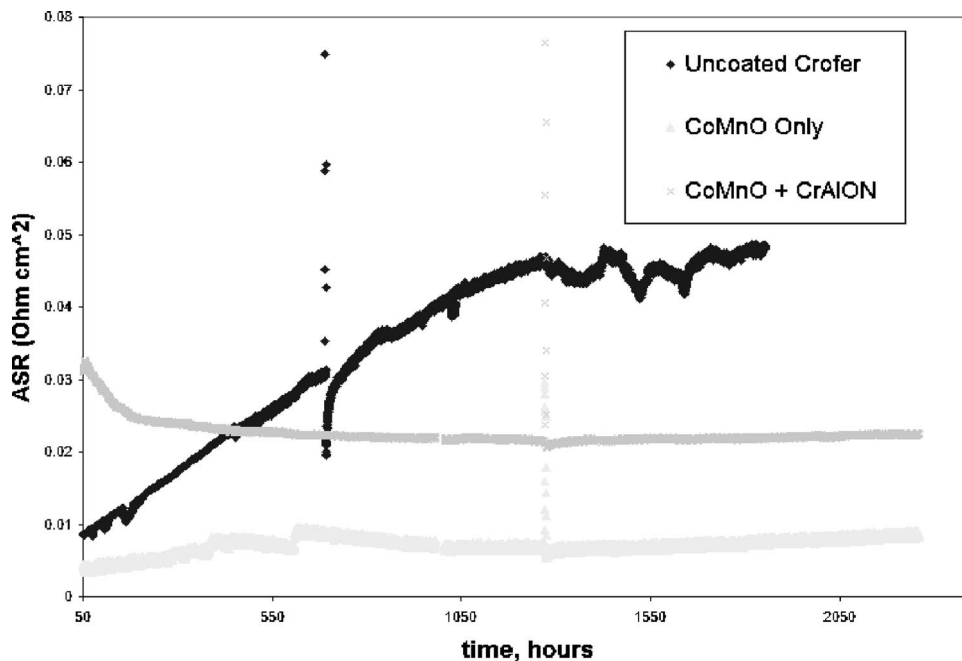
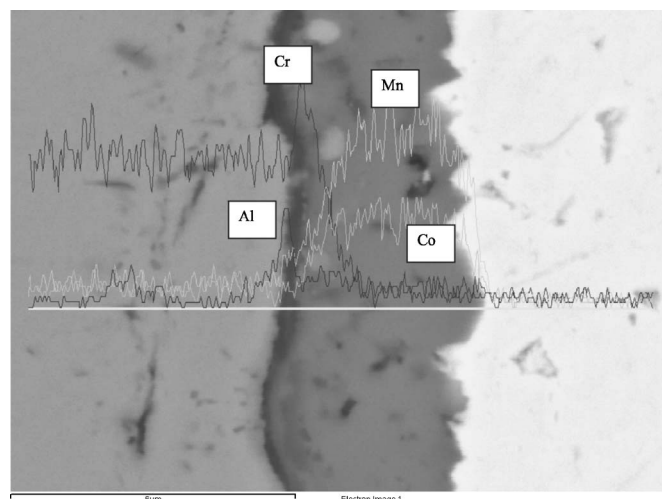


Figure 7. ASR testing results from MSU.



**Figure 8.** SEM/EDS cross section of dual segment coating after 200 h oxidation in air at 800°C.

The gradual decrease in ASR observed in the dual segment coating is likely due to interfacial and surface evolution during the test. ASR for both single and dual segment coated samples appear to rise after some time; however, the dual segment coating rises significantly slower. This is presumably due to the slower TGO scale growth of the dual segment coating compared with the single segment coating, which lacks the diffusion barrier attributes of the bond segment coating. In general, results from both PNNL and MSU ASR investigations are in good agreement, and indicate significant improvement afforded by the coatings studied here. Evidence for Ag paste interaction with both coated and uncoated samples during testing is currently under investigation.

An SEM image with EDS line profiles for individual elements of the dual segment coating after ~200 h oxidation in air at 800°C is shown in Fig. 8. The composition of the upper segment layer is 1:1-Mn:Co, with negligible Cr content. The coating appears dense and well-adhered to the substrate material. Co observed in the bottom coating segment can be attributed to both the LAFAD CoCrAlON coating deposition process and the inward diffusion from the upper FAD-EBPVD Mn-Co-O segment. In comparison,

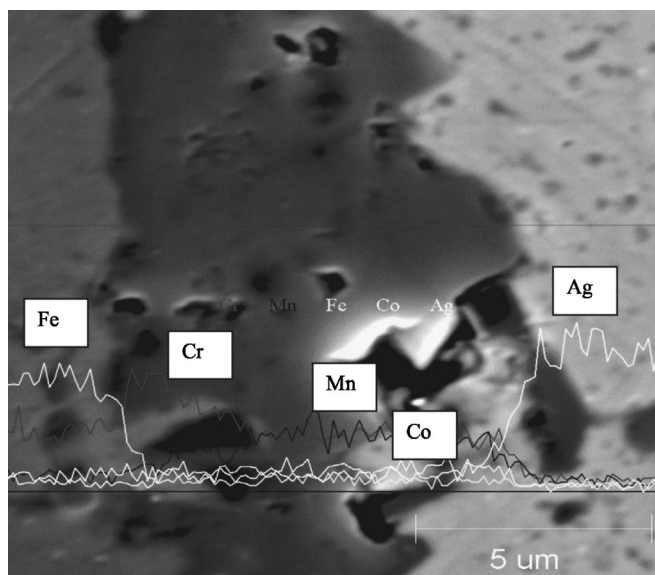


**Figure 9.** SEM/EDS cross section of dual segment coating after 800 h ASR testing with Ag contact.

Mn observed in the bottom segment can be attributed to the inward diffusion from the upper coating segment and outward diffusion from the Mn-containing Crofer substrate. The SEM cross section in Fig. 9 shows the dual segment coating after ASR testing for more than 800 h. EDS line scan results displaying elemental depth profiles overlay the SEM image. The coating thickness and composition before and after ASR testing remain similar and coating delamination was not observed. Again, negligible Cr content is found at top of the deposited layer, thus demonstrating the coating's effective reduction in Cr surface transport.

Figure 10 displays Cr volatilization results from single upper segment  $Mn_{1.5}Co_{1.5}O_4$  coated and uncoated Crofer 22 APU (results from the dual segment coating and bond coating alone are currently under evaluation). The single upper segment coated sample shows a 15-fold decrease in Cr volatility. SEM/EDS surface analyses after Cr volatility testing indicate that Cr-rich areas were present on uncoated areas (back side and near edges) of coated sample coupons. Coating

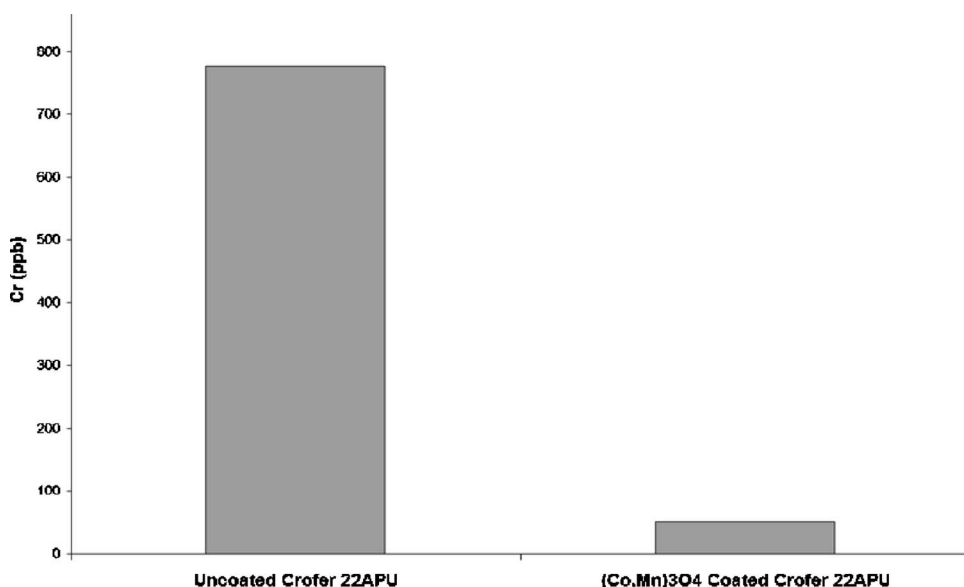


**Figure 10.** Cr volatility results from  $Mn_{1.5}Co_{1.5}O_4$  coated and uncoated Crofer 22 APU sample coupons.

damage and resulting Cr exposure is suspected to be caused by the Ni plating process for the uncoated side, as was readily observed in SEM/EDS analyses. Cr diffusion through the Ni plating is also unknown. Two-sided coated coupons are currently under investigation to mitigate these effects; however, these results do indicate a significant inhibition of Cr volatility compared with the uncoated steel.

### Conclusion

Coated and uncoated Crofer 22APU coupons have been investigated as function of exposure to SOFC-cathode gas phase conditions. The continued TGO scale growth observed on the uncoated coupons indicates their long-term incompatibility as SOFC interconnects. Improved long-term ASR stability and decreased Cr volatility of Crofer 22APU has been afforded by the use of two segment filtered arc Co-Cr-Al-O-N in addition to filtered arc assisted EB-PVD Mn-Co-O coatings. The observed improvement is likely the result of the diffusion-barrier characteristics of the lower segment coating and the high electrical conductivity and Cr-retention properties of the upper segment coating. Future work will focus on further enhancement of Crofer 22 APU and similar commercial ferritic steels through an extension of the basic coating system presented here.

### Acknowledgments

We acknowledge the technical assistance of Norm Williams, Lyman Fellows, and John Getty at Montana State University. Coatings were skillfully prepared by Duane Jones and Oleg Popov. Special thanks to Gerald Meier for fruitful discussion on oxidation kinetics. Portions of this work were supported by DOE under contract no. DE-FC26-04NT42225 and supervised by DOE project officer Travis Shultz. Work at MSU was supported through the High-Temperature Electrochemistry Center (HiTEC), supported by a DOI and DOE subcontract from PNNL, no. 3917(413060-A).

*Arcomac surface Engineering, LLC assisted in meeting the publication costs of this article.*

### References

1. S. C. Singhal and K. Kendall, *High-Temperature Solid Oxide Fuel Cells: Fundamentals, Design and Applications*, Elsevier Science, Ltd., New York (2004).
2. P. E. Gannon, C. T. Tripp, A. K. Knospe, C. V. Ramana, M. Deibert, R. J. Smith, V. I. Gorokhovskiy, V. Shutthanandan, and D. Gelles, *Surf. Coat. Technol.*, **188-189**, 55 (2004).
3. M. Williams and J. P. Strakey, in *Solid Oxide Fuel Cells VIII (SOFC VIII)*, S. C. Singhal and M. Dokiya, Editors, PV 2003-07, p. 3, The Electrochemical Society Proceedings Series, Pennington, NJ (2003).
4. Z. Yang, K. S. Weil, D. M. Paxton, and J. W. Stevenson, *J. Electrochem. Soc.*, **150**, A1188 (2003).
5. Crofer 22 APU MSDS No. 8005, June 2004, ThyssenKrupp VDM.
6. Z. Yang, J. S. Hardy, M. Walker, G. Xia, S. P. Simner, and J. W. Stevenson, *J. Electrochem. Soc.*, **151**, A1825 (2004).
7. V. Gorokhovskiy, U.S. Pat. 6,663,755 (2003).
8. V. I. Gorokhovskiy, R. Bhattacharya, and D. G. Bhat, *Surf. Coat. Technol.*, **140**, 82 (2001).
9. S. Elangovan, S. Balagopal, M. Timper, I. Bay, D. Larsen, and J. Hartvigsen, *J. Mater. Eng. Perform.*, **13**, 265 (2004).
10. Y. Yoo and M. Dauga, in *Solid Oxide Fuel Cells VII*, S. C. Singhal and H. Yokakawa, Editors, PV 2001-16, p. 837, The Electrochemical Society Proceedings Series, Pennington, NJ (2001).
11. N. Oishi, T. Namikawa, and Y. Yamazaki, *Surf. Coat. Technol.*, **132**, 58 (2000).
12. M. Kawate, A. K. Hashimoto, and T. Suzuki, *Surf. Coat. Technol.*, **165**, 163 (2003).
13. O. Banakh, P. E. Schmidt, R. Sanjines, and F. Levy, *Surf. Coat. Technol.*, **163**, 57 (2003).
14. S. PalDey and S. C. Deevi, *Mater. Sci. Eng., A*, **342**, 58 (2003).
15. Y. Larring and T. Norby, *J. Electrochem. Soc.*, **147**, 3251 (2000).
16. Z. Yang, G. Xia, and J. W. Stevenson, *Electrochem. Solid-State Lett.*, **8**, A168 (2005).
17. X. Chen, P. Y. Hou, C. P. Jacobson, S. J. Visco, and L. C. De Jonghe, *Solid State Ionics*, **176**, 425 (2005).
18. W.-D. Munz, T. Hurkmans, G. Keiren, and T. Trinh, *J. Vac. Sci. Technol. A*, **11**, 2583 (1993).
19. M. Mayer, Technical Report IPP 9/113, Max-Planck-Institut für Plasmaphysik, Garching, Germany (1997).
20. J. R. Tesmer and M. Nastasi, *Handbook of Modern Ion Beam Materials Analysis*, Materials Research Society, Pittsburgh, PA (1995).
21. R. J. Smith, C. Tripp, A. Knospe, C. V. Ramana, A. Kayani, V. Gorokhovskiy, V. Shutthanandan, and D. S. Gelles, *J. Mater. Eng. Perform.*, **13**, 295 (2003).
22. N. Birks, G. Meier, and F. Pettit, *Introduction to the High-Temperature Oxidation of Metals*, 2nd ed., Cambridge University Press, Cambridge (2006).
23. J. Beuth, Private communications, April 2006.